The Rho effector ARHGAP18 coordinates a Hippo pathway feedback loop through YAP and Merlin to regulate the cytoskeleton and epithelial cell polarity.

Emma C. Murray*, Gilian M. Hodge*, Leighton S. Lee, Cameron A.R. Mitchell, Andrew T. Lombardo

* These authors contributed equally to this manuscript.

The organization of the cell's cytoskeletal filaments is coordinated through a complex symphony of signaling cascades originating from internal and external cues. Two major actin regulatory pathways are signal transduction through Rho family GTPases and growth and proliferation signaling through the Hippo pathway. These two pathways act to define the actin cytoskeleton, controlling foundational cellular attributes such as morphology and polarity. In this study, we use human epithelial cells to investigate the interplay between the Hippo and Rho Family signaling pathways, which have predominantly been characterized as independent actin regulatory mechanisms. We identify that the RhoA effector, ARHGAP18, forms a complex with the Hippo pathway transcription factor YAP to address a long-standing enigma in the field. Using super resolution STORM microscopy, we characterize the changes in the actin cytoskeleton, on the single filament level, that arise from CRISPR/Cas9 knockout of ARHGAP18. We report that the loss of ARHGAP18 results in alterations of the cell that derive from both aberrant RhoA signaling and inappropriate nuclear localization of YAP. These findings indicate that the Hippo and Rho family GTPase signaling cascades are coordinated in their temporal and spatial control of the actin cytoskeleton.

Introduction

Extracellular signals are transduced through the cell membrane, in part through receptor ligand activation of Rho family GTPases. Rho family proteins bind and cycle between an active, guanosine triphosphate (GTP) bound, and an inactive guanosine diphosphate (GDP) bound state. This cycling has traditionally been referred to as a 'molecular switch' that turns on or off major actin regulatory components. These components include the actin-based molecular motor non-muscle myosin 2 (NM-2) through Rho Associated Kinase (ROCK) or the actin severing protein cofilin, through LIM kinase (Julian and Olson, 2014). Recent understanding has advanced the 'on/off' characterization of Rho GTPases to a more nuanced regulatory environment where both GTP and GDP bound states promote molecular interactions temporally and spatially (Denk-Lobnig and Martin, 2019). None-the-less, Rho family GTPases are well established as essential cellular signals for actin nucleation, polymerization, and organization into higher-order branched or bundled structures. These signals serve to order the cell into

polarized domains, defining the shape of the cell, the morphological structures present (e.g. microvilli, filopodia, etc.), and the cell-cell contacts required to build tissues.

Recently, a conserved mechanism of actin regulation has emerged where domain-specific regulation by Rho effectors is controlled on a minute temporal and spatial scale (Jackson et al., 2024; Landino et al., 2021; Swider et al., 2022). In Xenopus embryos, wounding results in the Rho-dependent reorganization of apical actin within 30 seconds (Sepaniac et al., 2023). In drosophila RhoA signaling precedes actin and myosin reorganization by only 4 seconds (Jackson et al., 2024). Our group recently characterized an epithelial specific RhoA signaling pathway involving ARHGHAP18 organizing at the apical surface of polarized cells on the scale of 100nm (Lombardo et al., 2024). Separately, we showed in human colorectal Caco2 cells that the RAB GAP Epi64A localizes to an approximately 75nm region at the base of microvilli to regulate the terminal web of actin controlling cell shape (Miller et al., 2022). Collectively, these findings indicate that from flies to humans, the cell regulates Rho family GTPases on the scale of each individual actin structure to build the correct structure at the correct time. In the progress of our studies, we discovered an unexpected phenotype in cells genetically lacking ARHGAP18. These cells exhibited a basal membrane actin phenotype opposite to what would be expected from the loss of a RhoA GAP, challenging the emerging model in the field.

ARHGAP18 shows a strong specificity for accelerating the hydrolysis of GTP of RhoA in epithelial cells (Maeda et al., 2011) but also exhibits increased activity toward RhoC in endothelial cells (Chang et al., 2014). RhoA-GTP regulates the actin cytoskeleton by promoting the activity of multiple downstream kinase pathways. Of these, two kinases are required for the formation of microvilli and apical actin organization in the polarized epithelial cells of the gut, kidney, and placenta: 1) ROCK regulates multiple separate cytoskeletal and NM-2 pathways, including phosphorylation myosin light chains (MLC) inducing the formation of bipolar contractile actin bundles. ROCK additionally activates the LIM kinase pathway, which phosphorylates cofilin, inactivating its actin severing and capping functions, resulting in longer actin filaments. 2) Lymphocyte Oriented Kinase (LOK) and its homologue STE20 Like Kinase (SLK) are activated upon binding to RhoA which phosphorylates a conserved ERM threonine (T567 in Ezrin) (Belkina et al., 2009; Pelaseyed et al., 2017). Phosphorylation opens ERMs liberating their F-actin and plasma membrane binding sites resulting in mechanical crosslinking between the actin cytoskeleton and the plasma membrane (Bretscher, 1983; Matsui et al., 1998). Active ERMs then feedback through direct binding to Rho family GTPase effectors to locally tune the Rho family GTPase signaling environment (Lombardo et al., 2024; Miller et al., 2022; Yeh et al., 2023; Zaman et al., 2021).

Through the downstream kinases, activated RhoA-GTP increases actin bundling in both stress fibers through NM-2 and microvilli through ERM activation in concert with

recruitment of additional microvilli specific components (Gaeta et al., 2021; Morales et al., 2023). RhoA GAPs limit these effects by accelerating the transition of RhoA, negatively regulating them toward its inactivated GDP-bound state. Thus, RhoA GAPs canonically reduce the formation of bundled stress fibers and microvilli core bundles in polarized epithelial cells. However, ARHGAP18 knockdown was reported to result in the disorganization of stress fibers in human cells (Lay et al., 2019). The fly homolog of ARHGAP18 was similarly reported to positively regulate Rho1 and was subsequently named conundrum (Conu) due to this unexpected phenotype (Neisch et al., 2013). Astonishingly, knockdown of ARHGAP18 in human 3D spheroids was reported to reduce MLC phosphorylation and resulted in a loss of stress fibers (Porazinski et al., 2015).

To explain these results, ARHGAP18 was hypothesized to act as a non-traditional RhoA GAP where genetic screening linked its enigmatic function to the cytoskeletal transcription factor Yes-associated protein (YAP) (Porazinski et al., 2015). A later study confirmed the association by identifying inappropriate YAP nuclear localization in ARHGAP18 deleted mice (Coleman et al., 2020). YAP and the transcriptional co-activator with PDZ-binding motif (TAZ) are the downstream effectors of the Hippo pathway. Hippo signaling originates with mechanosensation and nutrient availability at apical and junctional membranes in part through the ERM-related protein Merlin (also known as neurofibromin 2 or NF2) (Harvey et al., 2013; Reginensi et al., 2016). Hippo signaling shuttles YAP and TAZ between the cytoplasm and nucleus. When localized to the nucleus, YAP/TAZ promotes the activation of cytoskeletal transcription factors associated with cell proliferation and actin polymerization. Phosphorylation of YAP at the S127 residue results in targeting to the cytoplasm for eventual degradation (Zhao et al., 2010). The combined results of the studies linking ARHGAP18 to YAP/TAZ reported both upstream and downstream regulation, indicating a possible feedback loop. However, the mechanism of this potential relationship remained unknown.

In this manuscript, we characterize the aberrant actin networks of Jeg-3 human epithelial cells genetically lacking ARHGAP18. Using super resolution STORM to resolve the actin filament network to a resolution of <40nm, we report that loss of ARHGAP18 results in a near total loss of basal actin bundles, including stress fibers and filopodia. We characterize the alterations to the kinases downstream of RhoA signaling regulating basal actin organization. Our results indicate that the aberrant basal actin organization results from both RhoA regulation through canonical GAP activity and separately through ARHGAP18's regulation of YAP localization. We report that ARHGAP18 forms a stable complex with YAP, which regulates its cytoplasmic to nuclear shuttling to control basal actin organization. Further, ARHGAP18 binds to Merlin, enabling ARHGAP18 to act as a feedback system for the Hippo signaling pathway. This mechanism allows the cell to coordinate the Hippo and Rho family signaling pathways to regulate the actin cytoskeletal organization in response to both internal and external cues.

Results:

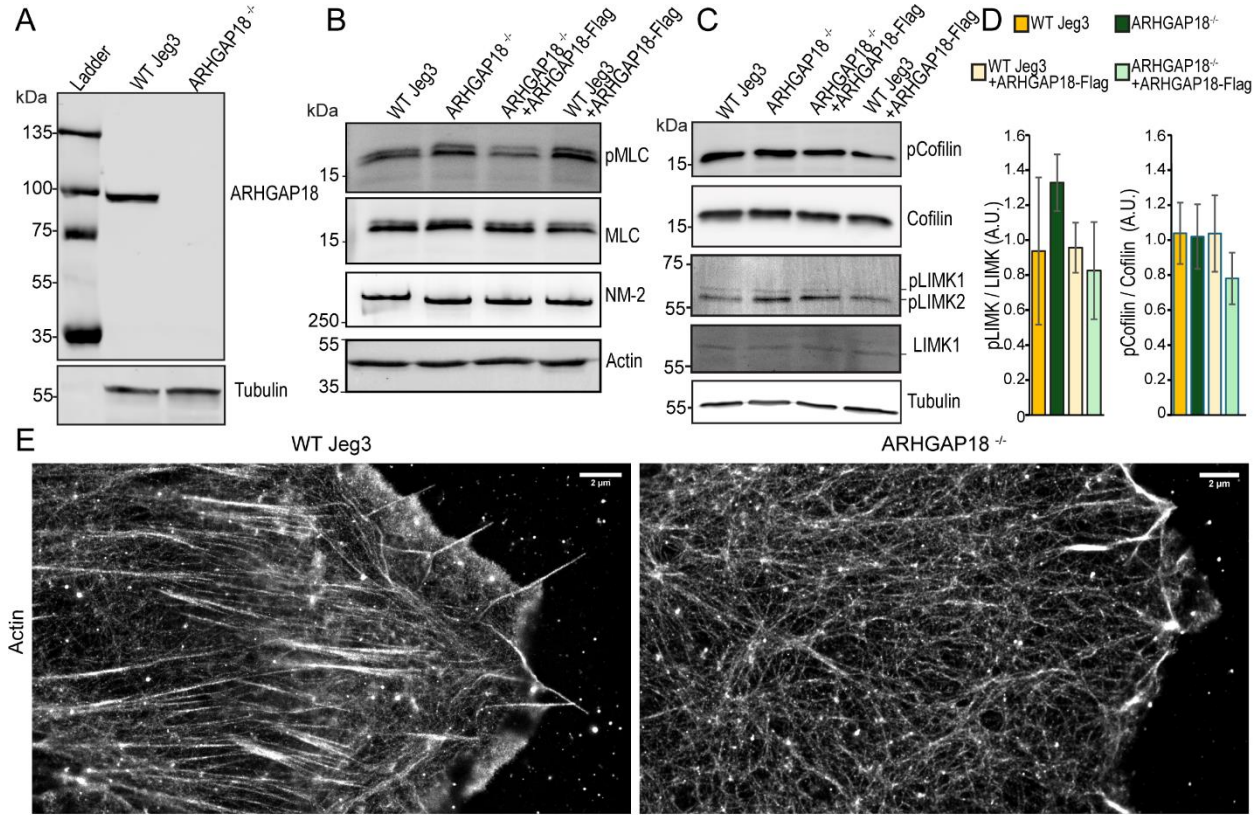

Figure 1: Characterization of ARHGAP18 Knockout in Human Epithelial Cells. A) Western blot of ARHGAP18 and Tubulin in WT Jeg-3 cells and ARHGAP18$^{-/-}$ knockout cells. B) Western blot of Non-muscle Myosin 2 (NM-2), Myosin Light Chain (MLC), and phosphorylated MLC (pMLC) in WT and KO cells with tagged ARHGAP18 rescue or overexpression. C) Western blot of total cofilin and LIM kinase vs. phosphorylated fractions of each in the same conditions as (B). Quantification of western blot intensity of the ratio of phosphorylated fraction over total for cofilin and LIMK in the conditions from (C). Bars indicate Mean±SEM; All conditions non-significant by t-test ($p>0.05$) n=3 E) STORM reconstructions of phalloidin stained Actin in fixed Jeg-3 WT and Jeg-3 ARHGAP$^{-/-}$ cells. Scale bar 2µm.

ARHGAP18 Regulates Non-Muscle Myosin-2 Through a RhoA Independent Mechanism

Our group recently characterized the regulation of microvilli through direct binding of ARHGAP18 to Ezrin, where we produced and validated CRISPR/Cas9 knock out of ARHGAP18 in human epithelial Jeg-3 cells (Fig. 1A) (Lombardo et al., 2024). In microvilli, ARHGAP18 acts to suppress active RhoA leading to reduced ROCK activation and lower MLC phosphorylation. Surprisingly, cells lacking ARHGAP18 and cells overexpressing ARHGAP18 both show increased phosphorylation of myosin light chain (Fig. 1B). Total expression levels of NM-2, total MLC, and actin are unchanged across these conditions (Fig. 1B). We hypothesized that the overexpression of ARHGAP18 was regulating the downstream RhoA kinase ROCK independent of its GAP activity. To probe this possibility,

we tested if the alternative signaling cascades downstream of ROCK were functioning properly. Using phosphospecific antibodies for western blotting, we detected that phosphorylation of LIM kinase (pLIMK) and cofilin (pCofilin) exhibited only minor changes in the absence of ARHGAP18 (Fig. 1C, D). While the abundance of phosphorylated LIMK appeared slightly increased in the KO cells, it did not rise to the level of statistical significance. Unlike pMLC, over-expression of ARHGAP18 resulted in only a modest decrease in phosphorylation of LIM kinase and Cofilin (Fig. 1D), which was not significantly different than WT cells. We concluded that ARHGAP18 was not a major regulator of LIMK or Cofilin activation. However, phosphorylation of MLC in the ARHGAP18 overexpression was regulated through a GAP-independent mechanism.

Cells Lacking ARHGAP18 have disorganized basal actin and a loss of focal adhesions

Increased pMLC in the absence of ARHGAP18 is expected to result in increased stress fiber formation through the activation of NM-2. However, multiple independent investigations, including our own, had identified the loss of stress fibers in cells with reduced or lacking ARHGAP18. To characterize the actin filament organization at the basal surface of cells lacking ARHGAP18, we employed Stochastic Optical Reconstruction Microscopy (STORM) to resolve the individual actin architecture to a spatial X-Y resolution of less than 40nm. WT Jeg-3 cells showed numerous stress fiber bundles at the basal surface of the cell (Fig. 1E). Actin filaments transitioned to lateral filaments running parallel to the plasma membrane and eventually to a canonical leading edge comprised of both cortical branched individual filaments and filopodia at the cell's plasma membrane. The orientation of the stress fibers and filopodia generally aligned in the axis going from cell center to cell exterior. In contrast to the WT actin organization, cells lacking ARHGAP18 exhibit a striking absence of both stress fibers and filopodia (Fig. 1E). The actin of ARHGAP18 KO cells was organized into small bundles and long individual filaments. Notably, the orientation of the ARHGAP18 KO cells' actin was substantially less aligned in the general axis going from cell center to cell exterior seen in the WT cells.

To further characterize the basal actin phenotype in cells devoid of ARHGAP18 further, we used immunofluorescent staining of NM-2B using spinning disk confocal. Stress fibers from WT cells showed actin colocalized with repeating striations of NM-2B indicative of active, contractile fibers (Fig. 2A). NM-2B still colocalized to actin in ARHGAP18 deficient cells but organized into smaller more diffuse puncta. We had previously reported that ARHGAP18-deficient cells were nearly twice as stiff as WT cells as measured by force indentation measurements using atomic force microscopy (Lombardo et al 2024). Given these data combined with our western blotting of pMLC, we concluded that NM-2B was still active in cells lacking ARHGAP18 and capable of forming

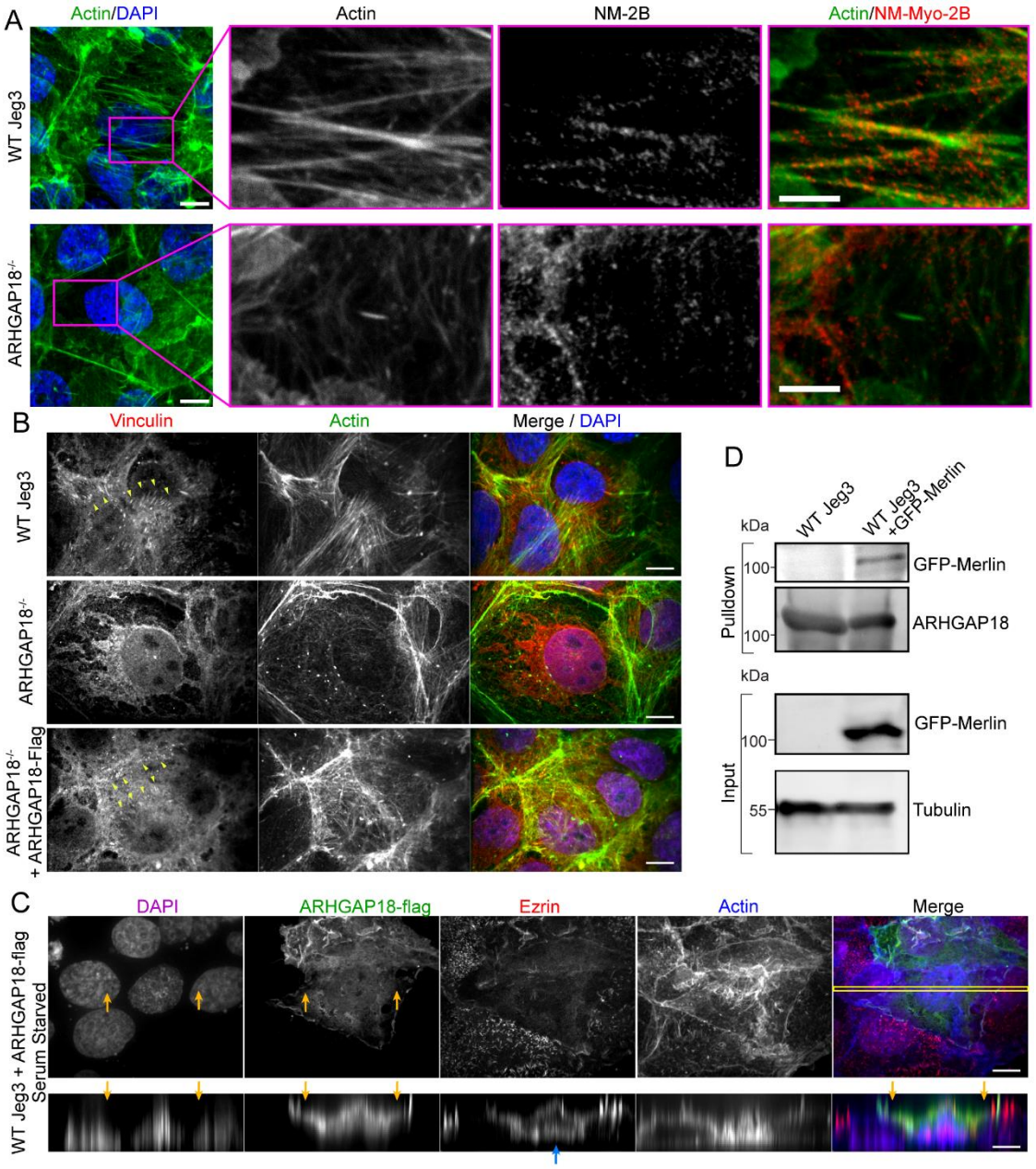

Figure 2: ARHGAP18 Binds Merlin and Effects NM-2 and Vinculin at the Basal Surface. A) Immunofluorescent imaging of actin and Non-Muscle Myosin-2B (NM-2B) in WT and ARHGAP18$^{-/-}$ cells. Scale bar 10μm; inset 5μm B) Immunofluorescent imaging of vinculin and actin in WT and ARHGAP18$^{-/-}$ cells and ARHGAP18-flag rescue cells. Focal adhesions co-localizing actin and vinculin highlighted with yellow arrowheads. Scale bar 10μm. C) Spinning disk confocal immunofluorescent imaging of WT Jeg-3 cells overexpressing ARHGAP18-flag. Actin to plasma membrane crosslinker ezrin localizes exclusively to the apical plasma membrane. Lower image row shows the X-Z dimension of the same image showing the invasion of the overexpressing cell onto neighboring cells. Yellow arrows indicate the sections of he overexpressing cell invading over neighboring cells' nucleus. Blue arrow indicates two stacked apical membranes by ezrin staining with the lower membrane from WT cells underneath the upper membrane from an ARHGAP18 overexpressing cell. Scale bars 10μm. D) Western blot of an ARHGAP18 pulldown from WT Jeg-3 cells with or without expression of GFP-merlin.

into contractile bundles but that the force-producing activity was not organizing the actin into large stress fiber bundles seen in the WT cells.

To investigate why basal actin organization was disrupted despite the activation of NM-2 in ARHGAP18 KO cells, we investigated the presence of actin to basal-membrane contact proteins. Immunofluorescent imaging of Vinculin in WT cells indicated that stress fibers were indeed tethered to the plasma membrane at the basal surface (Fig.2B). Imaging of ARHGAP18 $^{-/-}$ cells showed mislocalization of vinculin with no focal adhesions observed. Expression of full-length human ARHGAP18-flag in ARHGAP18$^{-/-}$ cells rescued both actin basal actin bundles and vinculin focal adhesion localization (Fig 2B). We sought to characterize the defects of pMLC overactivation and vinculin mislocalization in cells overexpressing ARHGAP18-flag. However, we discovered that WT cells overexpressing ARHGAP18 would often break from the surrounding Jeg-3 cell's monolayer to form three-dimensional stacks of cells (Fig. 2C). This characteristic was not typically seen in monolayered WT and ARHGAP18$^{-/-}$ cells (Fig. 2A). To investigate this invasive phenotype, we used transient transfection of ARHGAP18-flag into WT cells which allowed us to compare the behavior of WT cells side-by-side with ARHGAP18 overexpressing cells. Spinning disk confocal Z-dimensional slicing of the actin on these cells indicated that large basal actin bundles and stress fibers were present in the ARHGAP18 overexpression cells (Fig. 2C). We observed that cells overexpressing ARHGAP18 invade their neighboring cells monolayer climbing almost entirely on top of the adjacent WT cells (Fig. 2C yellow arrows). These data support the conclusion that ARHGAP18 acts to regulate basal and junctional actin through Rho-independent mechanisms.

ARHGAP18 regulates YAP phosphorylation and nuclear localization

Multiple prior studies indicated that ARHGAP18 interacts downstream of YAP through the Hippo pathway to regulate transcription of actin organization and cell proliferation. We hypothesized that the aberrant actin organization observed in ARHGAP18$^{-/-}$ cells, along with the invasive properties of overexpressing cells, resulted from a partial loss of the terminally differentiated apical/basal polarity characteristic of microvilli expressing cells. One possibility was the direct binding of ARHGAP18 to YAP or TAZ. A second possibility was that ARHGAP18 could influence YAP through upstream Hippo pathway components. Our group recently identified a short binding motif of ARHGAP18 from V10 to S17 that bound directly to the FERM domain of ERMs (Lombardo et al 2024). Merlin, which localizes to cell-cell junctions, acts upstream of YAP through the Hippo pathway shares a close structural similarity to ERMs. We tested if ARHGAP18 could form a complex with Merlin using a pull-down approach by passing lysate from WT Jeg-3 cells expressing a tagged Merlin construct over an immobilized ARHGAP18 column. We found that Merlin expressed in human Jeg-3 cells bound to the ARHGAP18 column (Fig. 2D). To investigate this interaction, we sought to identify if ARHGAP18 localized to

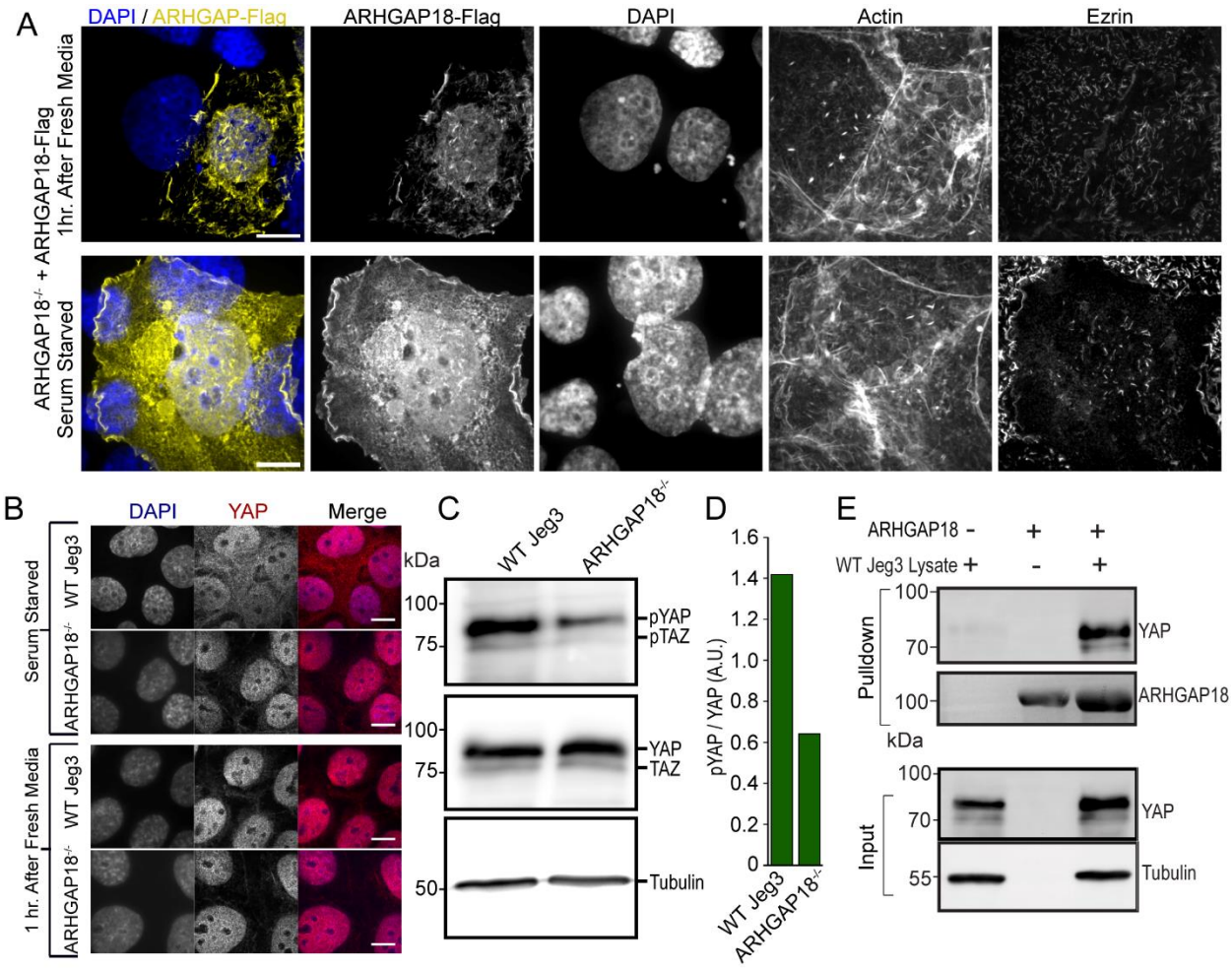

Figure 3: ARHGAP18 Binds Merlin and Effects NM-2 and Vinculin at the Basal Surface. A) Immunofluorescent imaging of ARHGAP18-flag rescue of ARHGAP18$^{-/-}$ cells in the serum starved or 1 hour after reintroduction of serum. ARHGAP18's localization includes the cytoplasm in the serum starved state. Ezrin staining of microvilli shows lower levels of microvilli in both conditions. Scale bar 10μm B) Immunofluorescent imaging of YAP in WT and ARHGAP18$^{-/-}$ cells in the serum starved state or 1 hour after reintroduction of serum. YAP localization to the cytoplasm during serum starvation is lost in ARHGAP18$^{-/-}$ cells. Scale bar 10μm C) Western blot of lysate from WT or ARHGAP18$^{-/-}$ cells shows a decrease in the phosphorylation of YAP and TAZ (pYAP/ pTAZ) in the knockout cells. D) Quantification of the band intensity of pYAP/YAP from the blot shown in (C). E) Pulldown experiment using an ARHGAP18-agarose column. YAP does not bind to the column agarose alone nor is YAP present on the purified ARHGAP18 column before the addition of WT Jeg-3 lysate. When Jeg-3 lysate passed over the ARHGAP18 column endogenous YAP stably binds.

junctions where Merlin is active. We used the rescue of ARHGAP18 $^{-/-}$ cells with a flag tagged ARHGAP18 to image the localization of ARHGAP18 in serum-starved versus cells supplemented with FBS for 1 hour following serum starvation (Fig. 3A). Maximum projection images of ARHGAP18-flag showed localization of ARHGAP18 to microvilli at the apical surface, along with the rescue of increased microvilli formation in ARHGAP18$^{-/-}$ cells as we've previously reported (Fig. 3A) (Lombardo et al., 2024). Additionally, ARHGAP18 localized strongly to the nucleus and junctions while being almost entirely excluded from the cytoplasm. Hippo pathway signaling responds to multiple external cues, including nutrient availability to signal downstream transcription for cell proliferation and cytoskeletal remodeling. When cells were deprived of serum, ARHGAP18's localization shifted to include substantial cytoplasmic staining (Fig. 3A). Interestingly, ARHGAP18's localization to microvilli and its reduction of the formation of microvilli was maintained in both conditions, indicating that the microvilli specific functions were independent from nutrient availability. We concluded that ARHGAP18 acted in part through a molecular interaction with Merlin at junctions. However, the results also indicated that ARHGAP18 may have a secondary, nuclear and cytoplasmic regulatory function depending on nutrient availability.

In serum-starved WT cells YAP is phosphorylated and localized to the cytoplasm (Zhao et al., 2010). Upon reintroduction of nutrients, YAP phosphorylation is reduced, and it is shuttled to the nucleus, where it acts to promote cell proliferation and actin polymerization. Next, we tested if YAP shuttling between the nucleus and cytoplasm in response to nutrient availability was altered in Jeg-3 cells lacking ARHGAP18. We used immunofluorescent staining of YAP in cells fixed in either serum-fed or serum-starved states. In WT serum-starved cells, YAP showed diffuse staining throughout the cytoplasm and nucleus (Fig. 3B). Upon reintroduction of serum into the media, YAP's cytoplasmic localization was lost within one hour, and only nuclear staining remained. In ARHGAP18 $^{-/-}$ cells YAP remained predominantly in the nucleus in both the serum-starved and serum-present media states. Using lysates from the serum-starved cells, we tested by western blotting the phosphorylation state of YAP and TAZ (Fig. 3C). While the total expression of YAP and TAZ remained the same in WT and ARHGAP18 KO cells, the phosphorylation of YAP and TAZ was reduced in the cells lacking ARHGAP18 compared to WT levels.

We hypothesized that ARHGAP18 may also form a complex with YAP that influences YAP's cytoplasmic localization. To test this hypothesis, we passed WT Jeg-3 lysates over the immobilized ARHGAP18 column to probe for binding of native proteins to ARHGAP18. We detected that endogenous YAP from WT Jeg-3 cells bound to immobilized ARHGAP18 (Fig. 3D). We concluded that YAP's localization to the cytoplasm in the serum starved state depended on the formation of a complex including both YAP and ARHGAP18. The combined results indicate that ARHGAP18 acts as both a negative

RhoA regulator and as part of a Hippo signaling feedback loop between YAP and Merlin to control polarized actin cytoskeletal structures.

Discussion:

Humans have 20 Rho family of GTPase genes where nucleotide state transitions are accelerated by a plethora of guanine nucleotide exchange factors (GEFs) and GTPase Activating Proteins (GAPs). This genetic complexity combined with partial overlapping molecular functions, has presented significant challenges to the characterization of the molecular functions of individual GAPs and GEFs in humans. For example, of the approximately 83 GEFs in humans, at least 24 have specific or partial activity for a single GTPase, RhoA (Vigil et al., 2010). Humans also have genes for three dissociation inhibitors (RhoGDIs), which regulate Rho family localization through membrane binding. Thus, much of our foundational understanding derives from careful experimentation in more genetically advantageous model systems (Etienne-Manneville and Hall, 2002). Here, we use CRISPR KO of human epithelial cells to investigate the loss of a single RhoA effector, ARHGAP18. We uncover that ARHGAP18 forms complexes with YAP and Merlin. These results indicate that Rho family effectors have the potential to act in complex and multifaceted cellular functions linking multiple signaling and polarity-driving pathways.

Regardless of the genetic background, a major technical challenge for the study of Rho-dependent signaling pathway's regulation of cellular actin architecture is that 1) actin is the most abundant protein in the cytosol, 2) actin forms three-dimensional interwoven webs of densely packed networks, 3) filaments can turn over on the scale of 30-60 seconds, and 4) the single filament structure is 7 nanometers across (two orders of magnitude below the diffraction limit of visible light). The advent of super-resolution STORM imaging has opened the door to fluorescent characterization of individual Rho family effectors on the actin cytoskeleton at the single filament level (Xu et al., 2012). While multiple prior studies have observed the change in actin bundles of cells with altered ARHGAP18 levels (Coleman et al., 2020; Neisch et al., 2013; Porazinski et al., 2015), our super resolution characterization allows for the dissection of the exact actin structures lost. Reorganization toward branched or individual filaments would dramatically alter the transport of polarity driving cargos by myosin and microtubule-based motors (Bensel et al., 2024; Heaslip et al., 2014; Lombardo et al., 2017; Lombardo et al., 2019). Our STORM data indicate that not all actin or all bundles are lost as it appears by our own traditional confocal staining (Compare Fig. 2A to Fig.1E). Instead, significant quantities of single filaments are maintained in areas that appear devoid of actin. This, in and of itself, is a notable point that should be considered when describing actin organization using conventional light microscopy. In short, most actin seen on a traditional light microscope is a bundle. Our data indicates that the loss of ARHGAP18

switches the epithelial cell's basal actin signaling toward a state where the actin architecture resembles a leading edge comprised of single and branching filaments.

With the data presented here we find the naming of the fly ortholog of ARHGAP18 as conundrum (Conu) appropriate. Our results add to multiple prior reports indicating that ARHGAP18 has additional cellular functions outside of Rho GAP activity (Coleman et al., 2020; Lay et al., 2019; Neisch et al., 2013; Porazinski et al., 2015). ARHGAP18 was first identified as a novel Rho effector in a microarray screen of proteins regulating capillary tube formation by human umbilical vein endothelial cells (Coleman et al., 2010). The fly ortholog conundrum (Conu) was subsequently reported to localize to the cell cortex through a molecular interaction with the only fly ERM, Moesin (Neisch et al., 2013). However, increased expression of Conu did not produce a phenotype typical of reduced levels of Rho1 as expected from a GAP and instead led to proliferation and cell overgrowth. We identify the same unexpected phenotype in our ARHGAP18 overexpression in human epithelial cells, where cells invade into neighboring monolayers (Fig. 2C).

ARHGAP18$^{-/-}$ cells exhibiting a near total loss of stress fibers (Fig. 1E) despite increased cellular levels of pMLC (Fig. 1B) (Lombardo et al., 2024) represents the strongest argument that ARHGAP18 functions in alternative pathways to RhoA/C alone. Our data raises several questions about how Rho and YAP are coordinated: First, what is the effect of ARHGAP18 complexing with both Merlin and YAP? Loss of ARHGAP18 results in increased active RhoA at junctions (Lombardo et al., 2024) promoting apical actin reorganization. Thus, it's reasonable to conclude that one of Merlin's functions as a scaffolding protein is to sequester ARHGAP18 to junctions to regulate RhoA locally. When nutrients are low, merlin is inactivated and dissociates from the junctional cytoskeletal structures (Bretscher et al., 2002; Gladden et al., 2010). Inactivation of Merlin would mask the predicted binding site for ARHGAP18 in the conserved FERM domain shared with ERMs. ARHGAP18 would then be free to complex with YAP in the cytosol. The shuttling we characterize of ARHGAP18 localizing from junctions to the cytoplasm in response to serum availability (Fig. 3A) matches this proposed mechanism. This system would place ARHGAP18 as a signaling link between the Hippo and RhoA cascades and as a component in a negative feedback loop between Merlin and YAP.

Second, why is NM-2 not producing bundles despite being active in cells lacking ARHGAP18? The parameter space for defining this phenotype makes experimentation extremely challenging as actin bundlers, nucleators, severing proteins, and polymerization effectors may all be affected by the alterations to YAP and RhoA in ARHGAP18$^{-/-}$ cells. The list of available mechanisms that YAP alone may induce under perpetual nuclear localization (Fig. 3B) is daunting (Pocaterra et al., 2020). However, in summation, YAP activation promotes a stem cell-like phenotype in nearly all cells (Mo et al., 2014). Predictive modeling from *in silico* simulations has been productive in defining

the minimum components needed to organize complex cytoskeletal behaviors (Landino et al., 2021; Walcott and Warshaw, 2022). This approach will likely be needed in future investigations to narrow the potential candidates preventing stress fibers formation in ARHGAP18$^{-/-}$ cells. Prior experimental work can also provide some clues to NM-2 overactivation resulting in a loss of actin bundles. In microvilli, the loss of ARHGAP18 results in overactivation of apical NM-2 where motors produce enough force to shred the actin bundles of microvilli (Lombardo et al., 2024). This mechanism occurs to a lesser extent in the apical terminal web of actin in WT epithelial cells through NM-2C (Chinowsky et al., 2020). The force required to dissociate individual actin filaments from a bundle crosslinked by alpha actinin (stress fibers) or fascin (filopodia) is unknown and will require careful *in vitro* biophysical assays using atomic force microscopy or optical tweezers to define.

Collectively, our results support a model where loss of ARHGAP18 depolarizes cells by dysregulating apical, junctional, and basal membrane identification through ERMs, Merlin, and YAP respectively. The exact molecular interactors responsible for the signaling cascade that results in pMLC activation in the overexpression of ARHGAP18 will require future characterization. Further investigation of the molecular details of the ARHGAP18/YAP binding complex will elucidate the mechanism that ARHGAP18 uses to coordinate RhoA signaling with the Hippo pathway to define cell polarity and morphology.

Methods:

Reagents and cDNAs

Anti-ezrin antibody (CPTC-ezrin-1 supernatant concentrate obtained from the Developmental Studies Hybridoma Bank; catalog no. CPTC-Ezrin-1; Research Resource Identification AB_2100318) was used 1:100 for immunofluorescence. Mouse anti-Flag (Sigma-Aldrich; catalog no. F1804) was used at 1:250 for immunofluorescence and 1:5,000 for Western blot, and mouse anti-tubulin (Sigma-Aldrich; catalog no. T5168) was used at 1:5,000 for Western blot. anti-MLC2 (catalog no. 3672) and anti–phospho-MLC2 (phospho-Thr18/Ser19; catalog no. 3674) were purchased from Cell Signaling Technology and used at 1:500 in Western blots. Anti–nonmuscle myo-IIB from BioLegend (catalog no. 909902) and nonmuscle myo-IIA (BioLegend; catalog no. 909802) were used at 1:100 in both Western blots and immunofluorescence. The rabbit ARHGAP18 antibody was produced and characterized previously (Lombardo et al., 2024) and used at 1:500 for western blotting. The rabbit anti-vinculin antibody was a kind gift of A. Bretscher and was described previously (Franck et al., 1990) and used at 1:200 for immunofluorescence. For actin staining, Alexa Fluor 647 phalloidin (Invitrogen; catalog no. A30107) was used at 1:250.

Human ARHGAP18 constructs were produced using polymerase chain reaction (PCR) with New England Biolabs (NEB) Phusion High-Fidelity PCR Kit (Cat# E0553L). cDNA of

ARHGAP18 was obtained off a construct originally derived from the Harvard Plasma Database (ID # HsCD00379004). NEB Monarch PCR & DNA Cleanup Kits (Cat# T1030S) and Thermo Scientific GeneJET Gel Extraction Kits (Cat# K0692) were used to purify PCR and Gibson Assembly products. DNA products were cloned into the mammalian expression vector PQCXIP using NEB Gibson Assembly cloning Kit (Cat# E5510S). transformations were done into OneShot TOP10 bacteria (Thermo Fisher; Cat# C404010), selected using ampicillin resistance, and then sequenced for verification. GFP-merlin was a gift of A. Bretscher and produced previously (Sher Bretscher Dev Cell 2012)

Western Blotting:

Western blot analysis of cell lysates was done using 4–12% Thermo Fisher bolt SDS-PAGE gels (Cat# NW04120). Gels were transferred to a polyvinylidene difluoride (PVDF) membrane using a BioRad Transblot Turbo (Cat# 1704150) and blocked with 5% milk in Tris Buffered Saline (TBS) + 0.5% Tween-20 (TBST). For detecting MLC and pMLC, 0.2-µm pore size PVDF (EMD Millipore; Immobilon-PSQ) was used. Primary antibodies were incubated with the membrane in TBST supplemented with 5% BSA either for 1 hr at room temperature or overnight at 4°C. Bands were detected with infrared fluorescent secondary antibodies (Invitrogen or LI-COR Biosciences; catalog nos. 926-32221 and 926-32210). Membranes were imaged using a Bio-Rad MP ChemiDoc. ImageJ intensity profile built-in toolset was used for western blotting quantification, which was then averaged, normalized, and plotted in Microsoft Excel.

Immunofluorescent Imaging:

Room temperature (23°C) fixed cell confocal imaging was done using a spinning-disk (Yokogawa CSU-X1; Intelligent Imaging Innovations) Leica DMi600B microscope with a spherical aberration correction device and either a ×100/1.46 NA Leica objective. Hamamatsu ORCA-Flash 4.0 camera metal-oxide semiconductor device was used to capture images, and Z-slices of acquired images were assembled using SlideBook 6 software (Intelligent Imaging Innovations). Maximum-intensity projections were assembled in SlideBook 6 or ImageJ and exported to Adobe Illustrator for editing. Vertical expansion of side projections was used to increase visual clarity of apical/basal localization. Widefield microscopy was performed using an inverted Leica DMi8 widefield microscope equipped with a Leica ×100 NA air objective, a Leica DFC 9000 GTC camera, Leica Application Suite X, and Leica adaptive focus control.

Immobilized ARHGAP18 pulldowns:

To determine the interaction between ARHGAP18 and Merlin or YAP, pulldown assays were performed using cell lysate from Jeg3 wildtype cells. Purified human ARHGAP18 was produced by bacterial expression of an N-terminal-SUMO-HIS-tagged protein purified using a NiNTA resin as described in (Lombardo et al., 2024). Transfections for

GFP Merlin were performed using PEI MAX polyethylenimine reagent (Polysciences; Cat# 24765). Cells were harvested with lysis buffer (25 mM Tris, 5% glycerol, 150 mM NaCl, 50 mM NaF, 0.1 mM Na3VO4, 10mM βGP, 0.2% Triton X-100, 250 mM calyculin A, 1 mM DTT, 1× cOmplete Protease Inhibitor Cocktail [Roche; Cat# 11836153001]) by scraping. Lysates were then sonicated, and centrifuged at 8000 × g for 10 min at 4°C. Before incubating with the cell lysates, SUMO-ARHGAP18 NiNTA beads were equilibrated and washed into lysis buffer. The sample of the supernatant was taken for input, then the rest was added to the SUMO-ARHGAP18 NiNTA beads and nutated for 3 hr at 4°C. After incubation, the beads were pelleted and washed four times with a 2 minute incubation before boiling in 40 µL 2× Laemmli sample buffer.

Cell culture and expression vectors:

Jeg3 cells were purchased from ATCC.org (Cat# Htb-36) and maintained in a humidified incubator at 37°C and 5% CO2. Media for Jeg3 cells used in 1× MEM (Thermo Fisher Scientific; Cat# 10370088) with penicillin/streptomycin (Thermo Fisher Scientific; Cat# 15070063), 10% fetal bovine serum (FBS; Thermo Fisher Scientific; Cat# 26140079), and GlutaMAX (Thermo Fisher Scientific; Cat# 35050061). Corning 100 × 20 mm Petri-style TC-treated culture dishes (Cat# 430167) were used for maintaining cultures. Transient transfections used a PEI MAX polyethylenimine reagent (Polysciences; Cat# 24765). All cell lines were checked for mycoplasma in regular intervals using DAPI staining. ARHGAP18 knockout cells were created and characterized (Lombardo et al., 2024). In summary of these methods, multiple CRISPR single-guide RNAs against the sequence 5′-CAGCGGCAAGGACCAGACCG-3′ or 5′-CAGCGGCAAGGACCAGACCG-3′ were cloned into puromycin-resistant pLenti-CRISPRV2 (Addgene; Cat# 49535) which was transfected into 293TN cells with psPAX3 and pCMV-VSV-G (a gift from Jan Lammerding, Weill Institute for Cell and Molecular Biology, Cornell University, Ithaca, NY) for 48–72 hr. Jeg3 cells were then transduced with virus supplemented with Polybrene to 8 µg/mL twice a day for 2 days, followed by puromycin selection at 2 µg/mL. Mixed populations of selected cells were single-cell sorted and then screened by western blotting. ARHGAP18 expression vectors were created and described in (Lombardo et al., 2024).

Super-Resolution STORM:

Jeg-3 cells were plated on 35 mm 1.5 high precision glass bottom MatTek dishes (Cat# P35G-0.170-14-C) and fixed and permeabilized using 2mLs of 0.3% glutaraldehyde and 0.25% Triton X-100 in cytoskeleton buffer (10 mM MES pH 6.1, 150 mM NaCl, 5 mM EGTA, 5 mM glucose, and 5 mM $MgCl_2$) for 1-2 min at room temperature. Initial fixation was followed by 2% glutaraldehyde in cytoskeletal buffer for 10 min at room temperature. The sample was then treated with 1mL 0.1% NaBH4 in Phosphate Buffered Saline (PBS) at pH 7.4 for 7 min to reduce background fluorescence. Actin was stained in phalloidin at a dilution of 1:250 overnight at 4°C. Slides were washed into 50mM Tris, pH 8.0, 10%

glucose, 10mM NaCl, 0.5mg/ml Glucose oxidase, 0.04 mg/ml catalase with 10% cysteamine by weight, and 1.5% 2-Mercaptoethanol (BME) by weight. Stochastic Optical Reconstruction Microscopy (STORM)(Rust et al., 2006) was performed using a Zeiss Elyra super-resolution inverted Axio Observer.Z1 microscope provided by Cornell University's Institute of Biotechnology Imaging Facility. Lasers emitting 405 and 640 nm wavelengths through a 100x/1.46 NA oil objective captured images on a pco.edge 5.5m camera. Exposure time ranged from 50 to 400 ms and was dependent on the sample and channel to optimize STORM reconstruction. A minimum of 100,000 images were used for each STORM processing using the Imagej ThunderSTORM toolset (Ovesny et al., 2014) or The Zeiss Zen built-in STORM reconstruction toolset and adjusting the filtering conditions to maximize the signal to noise of single actin filaments in reconstructions.

Statistical Methods:

Statistical comparisons were performed in Microsoft Excel. The type of statistical tests utilized, the configuration of error bars, and the number of independent data points (*n*) are detailed in the figure legends respective to the data tested. Nonparametric or parametric testing was justified through the assumption of the tested data to have a normal distribution or not.

Acknowledgements:

We thank A. Bretscher and R. Visawantha for their kind gift of the human ARHGAP18 plasmid. We thank A Martin for their critical comments on the data interpretation. Preliminary data was collected under National Institutes of Health grant R35GM131751 to A Bretscher. We thank A. Heaslip and N. Bouffard for their expertise in troubleshooting STORM. Super resolution microscopy was performed at both the Microscopy Imaging Center at the University of Vermont (RRID# SCR_018821), and the Cornell Institute of Biotechnology Imaging Facility supported by the National Science Foundation funding (1428922).

Belkina, N.V., Y. Liu, J.J. Hao, H. Karasuyama, and S. Shaw. 2009. LOK is a major ERM kinase in resting lymphocytes and regulates cytoskeletal rearrangement through ERM phosphorylation. *Proc Natl Acad Sci U S A*. 106:4707-4712.

Bensel, B.M., S.B. Previs, C. Bookwalter, K.M. Trybus, S. Walcott, and D.M. Warshaw. 2024. Kinesin-1-transported liposomes prefer to go straight in 3D microtubule intersections by a mechanism shared by other molecular motors. *Proc Natl Acad Sci U S A*. 121:e2407330121.

Bretscher, A. 1983. Purification of an 80,000-dalton protein that is a component of the isolated microvillus cytoskeleton, and its localization in nonmuscle cells. *J Cell Biol*. 97:425-432.

Bretscher, A., K. Edwards, and R.G. Fehon. 2002. ERM proteins and merlin: integrators at the cell cortex. *Nat Rev Mol Cell Biol*. 3:586-599.

Chang, G.H., A.J. Lay, K.K. Ting, Y. Zhao, P.R. Coleman, E.E. Powter, A. Formaz-Preston, C.J. Jolly, N.I. Bower, B.M. Hogan, S. Rinkwitz, T.S. Becker, M.A. Vadas, and J.R. Gamble. 2014. ARHGAP18: an endogenous inhibitor of angiogenesis, limiting tip formation and stabilizing junctions. *Small GTPases*. 5:1-15.

Chinowsky, C.R., J.A. Pinette, L.M. Meenderink, K.S. Lau, and M.J. Tyska. 2020. Nonmuscle myosin-2 contractility-dependent actin turnover limits the length of epithelial microvilli. *Mol Biol Cell*. 31:2803-2815.

Coleman, P.R., C.N. Hahn, M. Grimshaw, Y. Lu, X. Li, P.J. Brautigan, K. Beck, R. Stocker, M.A. Vadas, and J.R. Gamble. 2010. Stress-induced premature senescence mediated by a novel gene, SENEX, results in an anti-inflammatory phenotype in endothelial cells. *Blood*. 116:4016-4024.

Coleman, P.R., A.J. Lay, K.K. Ting, Y. Zhao, J. Li, S. Jarrah, M.A. Vadas, and J.R. Gamble. 2020. YAP and the RhoC regulator ARHGAP18, are required to mediate flow-dependent endothelial cell alignment. *Cell Commun Signal*. 18:18.

Denk-Lobnig, M., and A.C. Martin. 2019. Modular regulation of Rho family GTPases in development. *Small GTPases*. 10:122-129.

Etienne-Manneville, S., and A. Hall. 2002. Rho GTPases in cell biology. *Nature*. 420:629-635.

Franck, Z., M. Footer, and A. Bretscher. 1990. Microinjection of villin into cultured cells induces rapid and long-lasting changes in cell morphology but does not inhibit cytokinesis, cell motility, or membrane ruffling. *J Cell Biol*. 111:2475-2485.

Gaeta, I.M., L.M. Meenderink, M.M. Postema, C.S. Cencer, and M.J. Tyska. 2021. Direct visualization of epithelial microvilli biogenesis. *Curr Biol*. 31:2561-2575 e2566.

Gladden, A.B., A.M. Hebert, E.E. Schneeberger, and A.I. McClatchey. 2010. The NF2 tumor suppressor, Merlin, regulates epidermal development through the establishment of a junctional polarity complex. *Dev Cell*. 19:727-739.

Harvey, K.F., X. Zhang, and D.M. Thomas. 2013. The Hippo pathway and human cancer. *Nat Rev Cancer*. 13:246-257.

Heaslip, A.T., S.R. Nelson, A.T. Lombardo, S. Beck Previs, J. Armstrong, and D.M. Warshaw. 2014. Cytoskeletal dependence of insulin granule movement dynamics in INS-1 beta-cells in response to glucose. *PLoS One*. 9:e109082.

Jackson, J.A., M. Denk-Lobnig, K.A. Kitzinger, and A.C. Martin. 2024. Change in RhoGAP and RhoGEF availability drives transitions in cortical patterning and excitability in Drosophila. *Curr Biol*. 34:2132-2146 e2135.

Julian, L., and M.F. Olson. 2014. Rho-associated coiled-coil containing kinases (ROCK). *Small GTPases*.

Landino, J., M. Leda, A. Michaud, Z.T. Swider, M. Prom, C.M. Field, W.M. Bement, A.G. Vecchiarelli, A.B. Goryachev, and A.L. Miller. 2021. Rho and F-actin self-organize within an artificial cell cortex. *Curr Biol*. 31:5613-5621 e5615.

Lay, A.J., P.R. Coleman, A. Formaz-Preston, K.K. Ting, B. Roediger, W. Weninger, M.A. Schwartz, M.A. Vadas, and J.R. Gamble. 2019. ARHGAP18: A Flow-Responsive Gene That Regulates Endothelial Cell Alignment and Protects Against Atherosclerosis. *J Am Heart Assoc*. 8:e010057.

Lombardo, A.T., C.A. Mitchell, R. Zaman, D.J. Mcdermitt, and A. Bretscher. 2024. ARHGAP18-ezrin functions as an autoregulatory module for RhoA in the assembly of distinct actin-based structures. *Elife*. 13.

Lombardo, A.T., S.R. Nelson, M.Y. Ali, G.G. Kennedy, K.M. Trybus, S. Walcott, and D.M. Warshaw. 2017. Myosin Va molecular motors manoeuvre liposome cargo through suspended actin filament intersections in vitro. *Nat Commun*. 8:15692.

Lombardo, A.T., S.R. Nelson, G.G. Kennedy, K.M. Trybus, S. Walcott, and D.M. Warshaw. 2019. Myosin Va transport of liposomes in three-dimensional actin networks is modulated by actin filament density, position, and polarity. *Proc Natl Acad Sci U S A*. 116:8326-8335.

Maeda, M., H. Hasegawa, T. Hyodo, S. Ito, E. Asano, H. Yuang, K. Funasaka, K. Shimokata, Y. Hasegawa, M. Hamaguchi, and T. Senga. 2011. ARHGAP18, a GTPase-activating protein for RhoA, controls cell shape, spreading, and motility. *Mol Biol Cell*. 22:3840-3852.

Matsui, T., M. Maeda, Y. Doi, S. Yonemura, M. Amano, K. Kaibuchi, S. Tsukita, and S. Tsukita. 1998. Rho-kinase phosphorylates COOH-terminal threonines of ezrin/radixin/moesin (ERM) proteins and regulates their head-to-tail association. *J Cell Biol*. 140:647-657.

Miller, M.R., D.J. McDermitt, C. Sauvanet, A.T. Lombardo, R. Zaman, and A. Bretscher. 2022. The RabGAPs EPI64A and EPI64B regulate the apical structure of epithelial cells. *Mol Biol Cell*. 33.

Mo, J.S., H.W. Park, and K.L. Guan. 2014. The Hippo signaling pathway in stem cell biology and cancer. *EMBO Rep*. 15:642-656.

Morales, E.A., I. Gaeta, and M.J. Tyska. 2023. Building the brush border, one microvillus at a time. *Curr Opin Cell Biol*. 80:102153.

Neisch, A.L., E. Formstecher, and R.G. Fehon. 2013. Conundrum, an ARHGAP18 orthologue, regulates RhoA and proliferation through interactions with Moesin. *Mol Biol Cell*. 24:1420-1433.

Ovesny, M., P. Krizek, J. Borkovec, Z. Svindrych, and G.M. Hagen. 2014. ThunderSTORM: a comprehensive ImageJ plug-in for PALM and STORM data analysis and super-resolution imaging. *Bioinformatics*. 30:2389-2390.

Pelaseyed, T., R. Viswanatha, C. Sauvanet, J.J. Filter, M.L. Goldberg, and A. Bretscher. 2017. Ezrin activation by LOK phosphorylation involves a PIP(2)-dependent wedge mechanism. *Elife*. 6.

Pocaterra, A., P. Romani, and S. Dupont. 2020. YAP/TAZ functions and their regulation at a glance. *J Cell Sci*. 133.

Porazinski, S., H. Wang, Y. Asaoka, M. Behrndt, T. Miyamoto, H. Morita, S. Hata, T. Sasaki, S.F.G. Krens, Y. Osada, S. Asaka, A. Momoi, S. Linton, J.B. Miesfeld, B.A. Link, T. Senga, N. Shimizu, H. Nagase, S. Matsuura, S. Bagby, H. Kondoh, H. Nishina, C.P. Heisenberg, and M. Furutani-Seiki. 2015. YAP is essential for tissue tension to ensure vertebrate 3D body shape. *Nature*. 521:217-221.

Reginensi, A., L. Enderle, A. Gregorieff, R.L. Johnson, J.L. Wrana, and H. McNeill. 2016. A critical role for NF2 and the Hippo pathway in branching morphogenesis. *Nat Commun*. 7:12309.

Rust, M.J., M. Bates, and X. Zhuang. 2006. Sub-diffraction-limit imaging by stochastic optical reconstruction microscopy (STORM). *Nat Methods*. 3:793-795.

Sepaniac, L.A., N.R. Davenport, and W.M. Bement. 2023. Bring the pain: wounding reveals a transition from cortical excitability to epithelial excitability in Xenopus embryos. *Front Cell Dev Biol*. 11:1295569.

Swider, Z.T., A. Michaud, M. Leda, J. Landino, A.B. Goryachev, and W.M. Bement. 2022. Cell cycle and developmental control of cortical excitability in Xenopus laevis. *Mol Biol Cell*. 33:ar73.

Vigil, D., J. Cherfils, K.L. Rossman, and C.J. Der. 2010. Ras superfamily GEFs and GAPs: validated and tractable targets for cancer therapy? *Nat Rev Cancer*. 10:842-857.

Walcott, S., and D.M. Warshaw. 2022. Modeling myosin Va liposome transport through actin filament networks reveals a percolation threshold that modulates transport properties. *Mol Biol Cell*. 33:ar18.

Xu, K., H.P. Babcock, and X. Zhuang. 2012. Dual-objective STORM reveals three-dimensional filament organization in the actin cytoskeleton. *Nat Methods*. 9:185-188.

Yeh, A.R., G.J. Hoeprich, B.L. Goode, and A.C. Martin. 2023. Bitesize bundles F-actin and influences actin remodeling in syncytial Drosophila embryo development. *bioRxiv*.

Zaman, R., A. Lombardo, C. Sauvanet, R. Viswanatha, V. Awad, L.E.R. Bonomo, D. McDermitt, and A. Bretscher. 2021. Effector-mediated ERM activation locally inhibits RhoA activity to shape the apical cell domain. *J Cell Biol*. 220.

Zhao, B., L. Li, K. Tumaneng, C.Y. Wang, and K.L. Guan. 2010. A coordinated phosphorylation by Lats and CK1 regulates YAP stability through SCF(beta-TRCP). *Genes Dev*. 24:72-85.